

Dynamics of supernova bounce in laboratory

S.I. Blinnikov,^{1,2,3,4,*} R.I. Ilkaev,^{5,†} M.A. Mochalov,^{5,‡} A.L. Mikhailov,^{5,§} I.L. Iosilevskiy,^{6,¶}
A.V. Yudin,^{1,**} S.I. Glazyrin,^{2,1,7,8,††} A.A. Golubev,^{1,8,‡‡} V.K. Gryaznov,^{9,§§} and S.V. Fortova^{10,¶¶}

¹*NRC “Kurchatov Institute” – ITEP, Moscow 117218, Russia*

²*Dukhov Research Institute of Automatics (VNIIA), Moscow 127050, Russia*

³*Kavli IPMU (WPI), Tokyo University, Kashiwa 277-8583, Japan*

⁴*Space Research Institute (IKI), RAS, Moscow 117997, Russia*

⁵*Russian Federal Nuclear Center VNIIEF, Sarov, Nizhni Novgorod region 607188, Russia*

⁶*Joint Institute for High Temperatures, Russian Academy of Sciences, Moscow 125412, Russia*

⁷*Sternberg Astronomical Institute, Moscow M.V. Lomonosov State University, Moscow 119234, Russia*

⁸*National Research Nuclear University MEPhI (Moscow Engineering Physics Institute), Moscow 115409, Russia*

⁹*Institute of Problems of Chemical Physics, Russian Academy of Sciences, Chernogolovka, Moscow region 142432, Russia*

¹⁰*Institute of Computer Aided Design, Russian Academy of Sciences, Moscow 123056, Russia*

We draw attention to recent high explosive (HE) experiments which provide compression of macroscopic amount of matter to high, even record, values of pressure in comparison with other HE experiments. The observed bounce after the compression corresponds to processes in core-collapse supernova explosions after neutrino trapping. Conditions provided in the experiments resemble those in core-collapse supernovae, permitting their use for laboratory astrophysics. A unique feature of the experiments is compression at low entropy. The values of specific entropy are close to those obtained in numerical simulations during the process of collapse in supernova explosions, and much lower than those obtained at laser ignition facilities, another type of high-compression experiment. Both in supernovae and HE experiments the bounce occurs at low entropy, so the HE experiments provide a new platform to realize some supernova collapse effects in laboratory, especially to study hydrodynamics of collapsing flows and the bounce. Due to the good resolution of diagnostics in the compression of macroscopic amounts of material with essential effects of nonideal plasma in EOS, and observed development of 3D instabilities, these experiments may serve as a useful benchmark for astrophysical hydrodynamic codes.

I. INTRODUCTION

Astrophysics gathers data mainly from observations with no hope for full-scale experiments under laboratory conditions [1–4], especially on supernovae – the most energetic events in the universe. Nevertheless, recent progress in high energy density laboratory experiments [1–4] allows us to simulate to some extent the conditions in astrophysics. The main sites of such experiments are cumulative high explosive (HE) generators [1–4], lasers [5, 6], pulsed high-current facilities (Z-machine) [1–3, 7, 8]. Here we consider the HE driver shock-wave generator employed at explosive facilities. The values of pressure most recently obtained there are at record highs for this type of experimental facility: pressure $P \sim 100$ Mbar is reached in hydrogen isotope deuterium [9] as we report here. Though it is significantly lower than the pressure inside exploding stars, these experiments provide compression of a macroscopic amount of matter at low entropy, leading to a shock wave bounce that corresponds to processes in core-collapse supernova explosions. Such a similarity appears due to the growth of the stiffness in the equation of state due to strong quantum degeneracy effects for the free-electron component of strongly nonideal deuterium plasma, an effect that is emphasized by low-entropy conditions. Thus these experiments provide a new platform to realize some supernova collapse effects in the laboratory.

*Electronic address: Sergei.Blinnikov@itep.ru

†Electronic address: ilkaev@vniief.ru

‡Electronic address: postmaster@ifv.vniief.ru

§Electronic address: staff@vniief.ru

¶Electronic address: iosilevskiy@gmail.com

**Electronic address: yudin@itep.ru

††Electronic address: glazyrin@itep.ru

‡‡Electronic address: alexander.golubev@itep.ru

§§Electronic address: grvk@fcp.ac.ru

¶¶Electronic address: sfortova@mail.ru

Supernova explosions represent one of the most energetic and exciting objects in the universe [2, 3, 10], which is why researchers are so interested in studying them. The records of those events are found in ancient chronicles during the millennia of written history, but the real scientific study of supernovae began only in 20th century. During the past few decades a lot of theoretical models have been proposed [10], none of which could describe all stages of this complex and extreme phenomenon.

At the same time, the general picture of the explosion is quite well established [10]. For initial stellar masses $\sim (10 - 25)M_{\odot}$, the explosion occurs due to core collapse. In a stationary star the internal pressure is exactly compensated by gravity. After exhaustion of nuclear fuel in the core of a star, the equation of state changes, leading to the decrease of the adiabatic exponent when the internal pressure is unable to resist the growth of the gravitational force in the core. This eventually leads to unimpeded compression or collapse. Unless another equation of state change happens, the process would go to infinity. In reality, at high density due to degeneracy and nonideality of plasma, the stiffness of the equation of state rises dramatically, which leads to the bounce of infalling matter and formation of the outgoing shock, which finally may produce the supernova explosion. This process is complicated by other physical effects, the most important of which is the generation of huge neutrino flux (see Sec. IV).

Today there is no hope to approach in the laboratory the ultraextreme conditions in plasma that appear in supernova explosions [1–4], but we try to qualitatively reproduce the hydrodynamical phenomena occurring in collapsing material: the effects of degeneracy, nonideal plasma and bounce. A similar physics appears in explosive experiments [11, 12] with deuterium plasma. Another benefit of these explosive experiments is in significantly lower values of specific entropy compared to laser. This feature is important for comparison with core-collapsing supernovae, where the values of entropy are also low.

The unique high energy laboratory experiments were specifically designed to reach high levels of pressure and density. These conditions are reached as a result of a special assembly: a multilayer system that maintains a quasi-isentropic regime of compression with low levels of entropy generation. The achievements of recent years in symmetry control of explosive compression allow us to reach high values of pressure. At the final stage the deuterium plasma has pressure $P = 114 \pm 20$ Mbar, and this is the record for shock-wave experiments with high explosives. Generation of high-pressure, high-temperature matter by multiple reverberating shock waves is well known [13–15] but is restricted by the pressure level $\sim 1 - 5$ Mbar.

This paper has the following structure. Section II discusses our HE experiments: the device and experimental results. Section III presents the equations of state that describe matter under extreme conditions in explosion experiments (but not in supernova (SN) explosions). Section IV presents our simulations of stellar collapse and describes the basic similarity between HE experiments and the core-collapse physics. In Sec. V we summarize our results and in Sec. VI we suggest a path for future work.

II. HIGH EXPLOSIVE EXPERIMENTS

A high explosive experiment that includes high pressure studies of matter needs a specially designed geometry. The target is a gas, surrounded by a shell-pusher, that is accelerated by high-explosives outside the shell. The installation is carefully adjusted with used explosive intensity in order to reach the effective compression of the target. Also a number of diagnostics are presented. The whole construction is schematically depicted in Fig. 1.

Using this construction we can observe various stages of plasma dynamics in the x-ray images like the one shown in the left panel of Fig. 2.

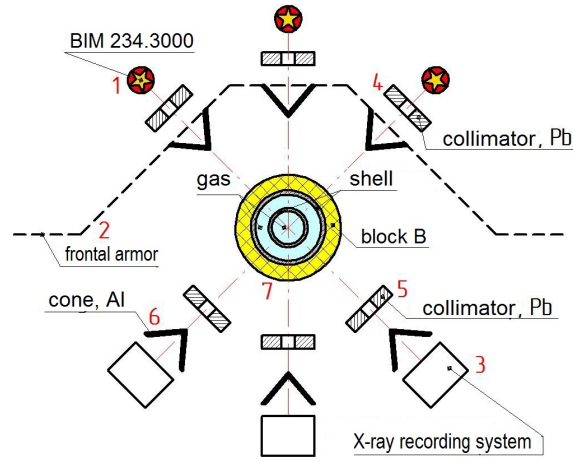


Figure 1: Schematics of experiment. 1, sources of x-ray radiation (betatrons); 2, shielding; 3, registrators; 4-5, collimators (Pb); 6, cone (Al); 7, target experimental device (working gas, shells, high explosive). This design is for a two-cascade device with the central block shown in Fig. 3. In the case of a single-cascade device the central block is simpler, cf. Fig. 2.

A. Single-cascade devices

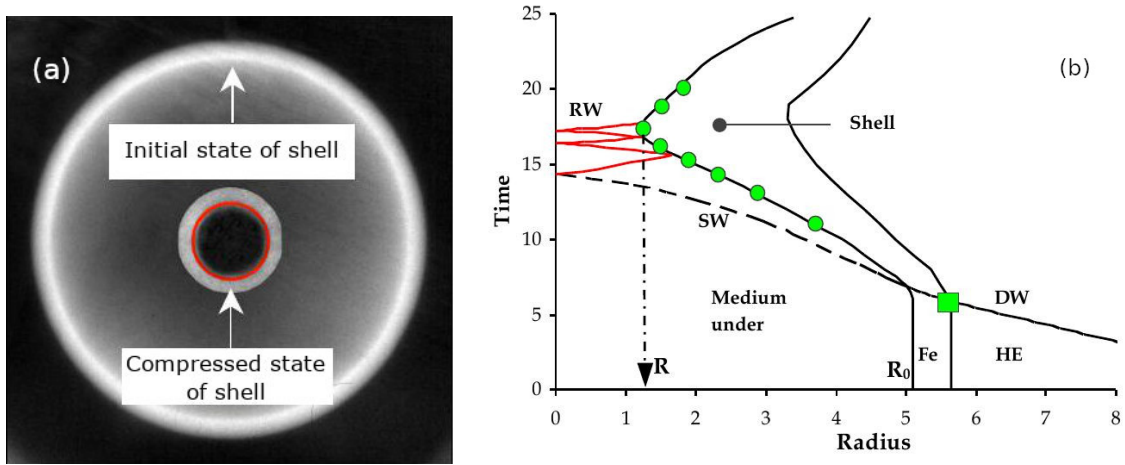


Figure 2: (a) x-Ray images of spherical device with a single-cascade scheme [16]. The image shows both the initial state and the maximum compression state. (b) Schematics of the single-cascade device dynamics. Circles (green online) show the positions of internal shell boundary measured in the experiment. The square dot shows the shell position measured by electrocontact technique. DW, detonation wave; SW, shock wave; RW, reverberating wave; HE, high explosive.

The simplest experimental device (“a single-cascade scheme”) for studying the compressibility of dense plasma is a gas-filled metal shell of spherical shape surrounded by a block of a HE. Schematically, the process of matter compression in such a construction is shown in Fig. 2 in the radius-time diagram. After the end of explosives detonation, a shock wave (SW) is formed in the metallic shell. Further, the SW enters the investigated substance. After its reflection from the center of the system and from the inner boundary of the moving shell a system of weak shock waves is formed in the region of the investigated substance (red lines) that compress and heat it up. Additional compression is provided by the shell smoothly converging to the center. Thus, the circulation of shock waves and smooth compression by the shell transform shock-wave compression into quasi-isentropic compression. In the final result, due to the growth of pressure inside the material being studied, the shell stops (at radius R in Fig. 2) and then bounces back. Smaller is the jump in entropy in the first and subsequent shock waves, closer the compression process approaches the isentropic one. In such systems, conditions for a longer retention of the matter at high pressure are more favorable as compared with loading by a single shock wave. With this loading method, various isentropes are achieved, with parameters depending on the mass of explosives and the geometry of the experimental devices. Those parameters can be changed

in a wide range. Such a single-cascade construction allows us to compress hydrogen to the density about 2 g/cm^3 by pressure $P \approx 1300 \text{ GPa}$ [17, 18]. A similar construction was used also in Ref. [16], where the deuterium plasma was compressed to the density of 4 g/cm^3 at pressure of 1800 GPa .

The physical picture developing in those experiments is rather simple. First, we have a fluid of neutral molecular hydrogen that is dissociated and ionized by the first and second shocks to almost ideal plasma. This stage is followed by the fast growth of Coulomb corrections in EOS of the compressed hydrogen (Coulomb nonideality) and electron degeneracy in the second, third, etc., shocks [1–4]. Finally, a transition to strongly degenerate nonideal plasma occurs. It should be noted that the degree of the Coulomb corrections is controlled by a special dimensionless parameter of nonideality [19–23],

$$\Gamma = \frac{(Ze)^2}{r_s kT} \approx \frac{e^2 n_e^{1/3}}{kT}, \quad (2.1)$$

where $Z = 1$ for hydrogen and r_s is the Wigner–Seitz radius, defined by

$$r_s = \left(\frac{3}{4\pi n_e} \right)^{1/3}. \quad (2.2)$$

The parameter Γ is equal to the ratio of the Coulomb interaction energy to the average kinetic energy of charged particles. The pressure correction due to electron degeneracy is controlled by another dimensionless parameter,

$$\xi = n_e \left(\frac{h^2}{2\pi m_e kT} \right)^{3/2} = n_e \lambda_e^3, \quad (2.3)$$

here $\lambda_e = (h^2/2\pi m_e kT)^{1/2}$, i.e., the thermal de Broglie wavelength. It should be noted also that the effect of electron degeneracy manifests itself in EOS via two channels: (i) the degeneracy of free (unbound) electrons, which is controlled by the parameter ξ , and (ii) an indirect effect due to the strong short-range repulsion of electrons localized within bound complexes (atoms, molecules, atomic and molecular ions etc). Consequently, the resulting thermodynamics of quasi-isentropically compressed gas is controlled by the competition of the two strong effects: the nonideality because of attraction due to the average Coulomb interaction and the repulsion due to the electron degeneracy. As a result, one can ensure that at certain stages of the steel shell — pusher compression the thermodynamic trajectory of the compressed gas (which mimics the “collapse” of a supernova core) enters the region of the soft EOS corresponding to a combined dissociation-ionization-driven (“plasma”) phase transition at $P \sim 1 - 2 \text{ Mbar}$ with the density jump $\sim 15 - 20\%$. This phase transition was discovered in explosive experiments about a decade ago [24] and has been many times confirmed [9, 16, 25, 26]. It should be stressed that some first indications on the possible existence of another ionization-driven phase transition with a very high value of the density jump are obtained at pressure $P \sim 50 - 100 \text{ Mbar}$ in the latest high-explosive experiments [9], see details in Sec. II D. During crossing of the two-phase region(s) of those phase transition(s) the EOS of the compressed deuterium becomes very soft, so that the rate of the shell braking by the pressure of the compressed gas goes down significantly (this mimics the “collapse”). The shell is still compressible (driven by products of the high explosion from outside) and is accelerating. At the moment when all of the deuterium goes into a close-packed phase of a strongly nonideal ($\Gamma \gg 1$) and strongly degenerate ($\xi \gg 1$) plasma, the rigidity and resistance of deuterium plasma, hence, the rate of the shell braking, increase sharply. This causes a “bounce” of the falling matter, and a shock at the bounce will run out into the shell.

B. Two-cascade devices

A new type of experimental spherical device with separated cavities was recently proposed to study the properties of plasma at high compression ratios. This so-called two-cascade device has been developed and is now being used to increase the compression ratio of plasma. The device is schematically shown in Figs. 1 and 3. The compression of the gas and plasma in such a construction is achieved by the action of steel spherical shells (1) and (2), see Fig. 3. The shells are accelerated to the center of symmetry of the device by the explosion of a powerful condensed explosive (3), made on the basis of octogen, and by a system of shock waves reverberating in the cavity of the shell. The inner cavity of the shell (2) is protected from the direct action of the explosive layer by the softening layer from the test gas, which largely eliminates the ejection of metal particles into the internal plasma cavity. To further reduce perturbations from the initiation system, a plexiglass gasket (4) is used between the explosive unit (3) and the outer shell (1).

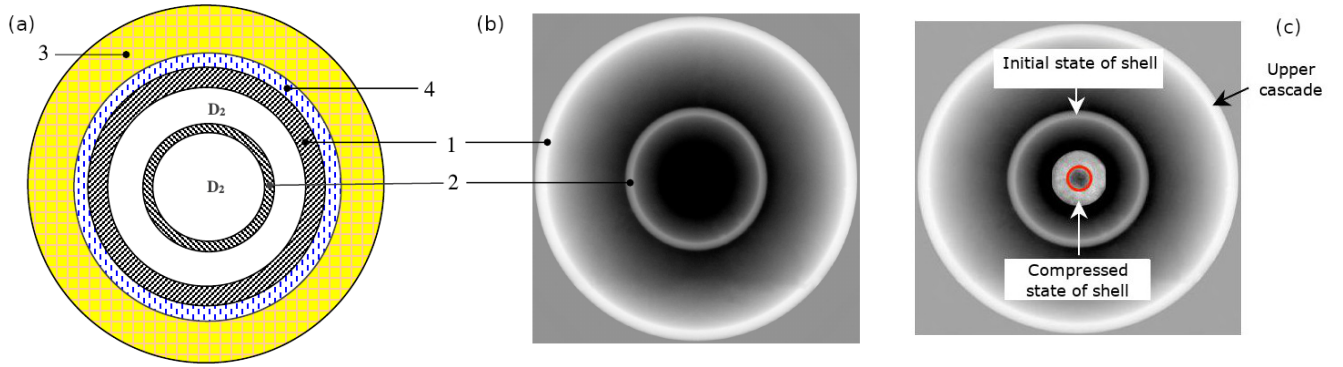


Figure 3: (a) A schematic design of a two-cascade spherical experimental device: 1, shell 1 (Fe1); 2, shell 2 (Fe2); 3, explosive, 4 – plexiglass; (b) x-Ray patterns (roentgenograms) of the shells in the initial state. (c) Initial and final states of the shell shown in one shot.

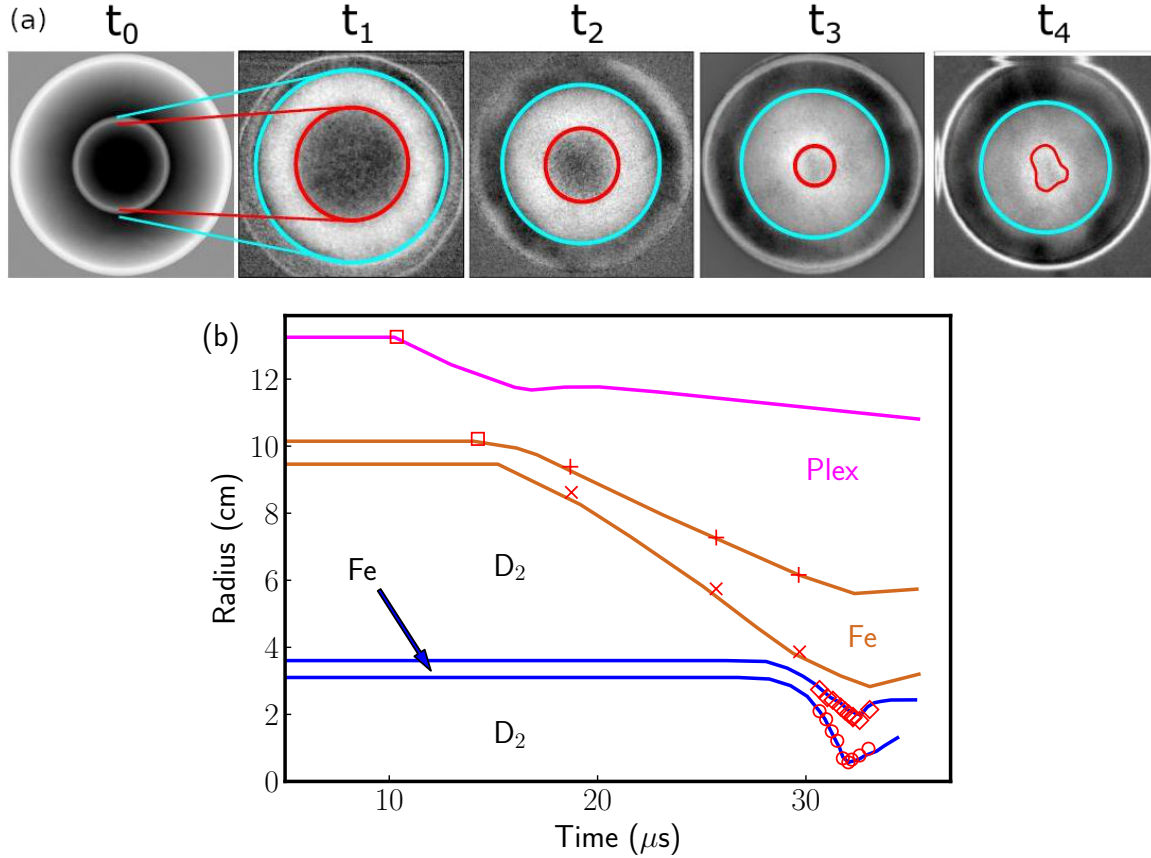


Figure 4: $R(t)$ diagrams for shells in the experimental device filled with deuterium which produced the record high compression. (a) x-Ray images of the shell 2 (see Fig. 3) as a function of time, where t_0 is the initial state, t_1 and t_2 are the compression phases, t_3 is the moment of maximum compression (“bounce”) and t_4 is the expansion phase; light and red circles are the outer and inner boundaries of the shell 2, respectively. (b) experimental data and calculated $R(t)$ diagrams, symbol \square denotes the results of electrocontact technique, symbols $+$ and \times are used for x-ray data from the model experiment, and symbols \diamond and \circ for the data of the basic experiment.

Using devices of this type, the compressibility of deuterium plasma in the pressure region up to $P \approx 5500$ GPa was investigated in Ref. [26]. At a ratio of the initial gas pressures in the inner and outer cavities $\approx 1 : 9$ with such a construction, a helium plasma was compressed in Ref. [25] by a factor of 600 with pressure $P \approx 3000$ GPa. A spherical device similar to that described in Ref. [26] was recently used in the experiment on the compression of deuterium plasma with pressure of 10^4 GPa [9] (those new experiments were proposed and discussed in Ref. [27]). To compress the deuterium plasma to these high values of pressure, a significant amount of explosives is required: $m \approx 85$ kg TNT.

A number of x-ray images (roentgenograms) obtained in the new experiment [9] is shown in Fig. 4.

To describe the process of plasma compression as a function of time, one needs to carry out reliable numerical simulations. The simulations must cover the propagation of shocks through the elements of the structure and the motion of the shells in the initial phase (when the effect of the gas is practically absent). To select the gas-dynamic codes for those simulations, a preliminary model gas-dynamic experiment was performed with a hemispherical block simulating the geometry of the structure and the technology of the full experiment. In the preliminary experiment, the propagation of shocks through the plexiglass (the motion of the shells in the initial phase) was recorded, and the velocity of the inner boundary of the shell 1 in Fig. 4 was measured.

The experimental data for the two-cascade device are shown in Fig. 4(b) together with the results of the gas-dynamic calculations. From the graph in Fig. 4(b), it can be seen that the gasdynamic calculation satisfactorily describes the control points of the shock motion: the data from the electroncontact technique in the plexiglass shell (symbol \square), the dynamics of the outer shell boundaries by x-ray images (symbols $+$ and \times) and the data of the basic experiment (\diamond and \circ). As follows from the analysis of the calculations performed, at the moment of the maximum compression in the deuterium plasma, the pressure has reached $P = (11400 \pm 2000)$ GPa and the temperature $T = 36\,500$ K with the measured density of the compressed plasma $\rho = 10.0 \pm 1.3$ g/cm³ and the compression ratio $\sigma = \rho/\rho_0 = 300$. The calculated value of the mean density $\rho_{\text{calc}} = 11.1$ g/cm³ agrees with the experimentally measured value within 11%. The criterion for the validity of the maximum pressure value obtained in this way is a good agreement between the experimental data and the calculated $R(t)$ diagram.

Our goal in the current paper is to point out from those laboratory experiments the physics that resembles supernova collapse. This is allowed due to the unique technique of generation and diagnostics of matter in the extreme states developed recently which allows matter compression by the energy of high explosive charges (see, e.g., Ref. [28] for a review).

As already mentioned, record levels of pressure in large volume ~ 50 Mbar [26] and a record compression ratio ($\rho/\rho_0 \sim 600$ [25]) have been achieved. Pressures $P \sim 100$ Mbar (in large volumes) have been achieved very recently [9], see Table.1.

C. Details of diagnostics used in the experiment

Very accurate simultaneity of initiation of the spherical and cylindrical high-explosive charges, achieved thanks to years of elaboration on this technique, provides a high degree of symmetry of the collapsing steel shell, which allows us to achieve a high degree of spherical symmetry of the material motion until the final moment of maximum compression of the sample (when density grows by a factor of hundreds). The symmetry of the driving shell is preserved until it stops before the ensuing “bounce”.

Extremely precise control of the parameters of the initial state is provided as well as control by X-ray patterns of the position of the moving (collapsing) shell, and parameters of the compressible material. The average density of the material is directly measured in the experiment from the position of the shell along its way until the time it stops just before its “bounce”.

The pressure of compressed plasma is extracted from sophisticated hydrodynamic calculations of the whole structure dynamics: the collapsing steel shell and the matter compressed in the shock-wave reverberations. The codes used in such simulations describe in needed detail the multicomponent dynamics of arbitrary matter phases: gases, solids, plasma, etc. The accuracy of the description was tested many times by comparison with experiments of similar type. The codes rely on sophisticated equations of state described below in Sec. III.

The quasi-isentropic compression of the target gas is achieved by a sequence of steps. The process starts by hitting the sample with an explosion-accelerated collapsing steel shell. The first shock converges toward the center and reflects there. After the reflection, a much weaker diverging shock appears, and then this shock is reflected by the steel shell, which is continuing to collapse. Then, again, even weaker shock converging toward the center propagates, etc., up to the moment of the final stopping of the shell.

Numerous calculations do show that the bulk of entropy growth occurs in the first shock wave. Further compression in a series of increasingly weak reverberating shocks can be treated as isentropic in good approximation. Hence, it was suggested to refer to this stage as *quasi-isentropic compression* [3, 17, 18].

Table II shows the main parameters achieved in various runs of high-explosive experiments. The most important quantity for comparison with core-collapsing supernovae is the specific entropy per baryon (the last column). It is close indeed to the predictions of the core-collapse simulations, see, e.g. Fig. 9.

To detect the position of the shells that compress the tested material, iron-free pulse betatrons (BIMs) are widely used in devices with large metal masses and high explosives [29, 30]. The average density of the compressed material is measured along the inner boundary of the shell with the plasma at the moment of its maximum compression (the “bounce” moment). Because the mass of the compressed matter is preserved, its density for a spherical device is

calculated from the following simple expression:

$$\rho = \rho_0 (R_0/R_{\min})^n, \quad (2.4)$$

where ρ_0 is the initial gas density, R_0 and R_{\min} are the inner shell radius in the initial state and at the moment of its “bounce”, respectively; and $n = 2$ or $n = 3$ for cylindrical or spherical geometry, respectively.

The scheme of the experiment on the modern x-ray radiographic complex is shown in Fig. 1, cf. Ref. [26]. A shadow image of the boundaries of the inner shell compressing the gas under investigation was obtained by simultaneously using bremsstrahlung of three powerful betatrons (1) with an electron limiting energy of ≈ 60 MeV located at 45° angles to each other in a protecting concrete structure (2). A feature of the radiographic complex is the possibility of each radiator to operate in a three-pulse mode, which allows one to register up to nine phases of the shell motion in one experiment and thus to trace the entire dynamics of the target compression. When studying the motion of the shell for each betatron, an individual optoelectronic detection system is used. The latter is activated synchronously with the betatron pulses, which makes it possible to obtain three independent x-ray images. To eliminate the effect of scattered radiation on highly sensitive recorders (3), the size of the recording field in each of the three projections is limited by the lead collimators (4). To protect the betatrons (1) and optoelectronic x-ray detectors (3), aluminum cones (6) are used. Single crystals of sodium iodide activated with tellurium NaI (Tl) \varnothing 150 mm ($\lambda_{\max} = 410$ nm, decay time 250 ns) and lutetium silicate LSO \varnothing 80 mm ($\lambda_{\max} = 420$ nm, decay time 50 ns) are used as gamma converters in this system.

For additional technical details on diagnostics see Ref. [9].

D. Experimental data

Figure 5 shows the experimental data that allow us to study equations of state and the dynamics of the multilayer system. The results of this and other experiments are shown in Table I and in Fig. 6. The data on the compressibility of deuterium plasma (obtained at pressure up to $P \approx 5500$ GPa from Ref. [26]) show the density jump with $(\partial P/\partial \rho)_S \approx 0$ in the range $\Delta \rho = 1.46 - 1.68$ g/cm³ registered at temperature $T \approx 3700$ K and pressure $P \approx 150$ GPa. There is also a change in the slope of the derivative $dP/d\rho$ after the density jump (regardless of the magnitude $\Delta \rho$ of this jump). These data are associated with a plasma phase transition [3, 24, 26]. The results of the current work and [9] indicate a new change in the slope of the derivative $dP/d\rho$ at densities above $\rho \sim 5$ g/cm³ in a compressed plasma of deuterium. Those results hint to a new phase transition at $\rho \sim 5$ g/cm³ that should be carefully studied in future work. The development of the necessary experimental devices for this study is not particularly difficult.

III. THERMODYNAMICS

The compressed matter is described by the SAHA-EOS model [31] and the corresponding SAHA-D code (see Ref. [26] and references therein) in terms of the so-called quasichemical representation (“chemical picture”), in other words, by the method of the “free energy minimization”. Mutual transformations of components are described according to the equations of chemical and ionization equilibrium (such as the Saha equation) with corrections for nonideality. A nontrivial point is that the hot, dense hydrogen plasma in experiments [9, 16–18] is strongly nonideal and strongly degenerate, i.e., the corresponding dimensionless parameters and corrections are not small. This is so for the Coulomb parameter $\Gamma \gg 1$, introduced in (2.1), and for the electron degeneracy parameter $\xi \gg 1$ in (2.3).

The most “rigorous” approaches, *ab initio*, or first principle EOS, based on the so-called quantum Monte Carlo (QMC) and quantum molecular dynamics (QMD) ones, claim to reach the status of a “numerical experiment”, although it remains to be seen whether they are accurate enough to describe real experiments. They are very time-consuming and cumbersome, even in the standard reference variant Vienna Ab initio Simulation Package (VASP), a plane wave density functional code for quantum molecular dynamics simulations, see, e.g., Ref. [35]. These methods allow one to calculate directly only a part of the thermodynamic quantities, the “summation” values of pressure $P(\rho, T)$ and internal energy $U(\rho, T)$. They do not produce directly the truly full set of thermodynamic quantities (entropy, free energy, and chemical potential). The VASP technique also predicts the dissociative-plasma phase transition (see, e.g., Ref. [36]). For the discussion of the possible analogies of experiments with core-collapsing SNe, this is important.

HE-driven experimental results in Ref. [26] and all the theoretical models (SAHA, DFT/MD, CH EOS, SESAME, Urlin [34]) account in some way for a phase transition of the 1st kind with a significant jump in density in the region of 1.5 – 4 Mbar.

The basic analogy, which can conceptually relate thermal and fluid dynamics in explosive experiments with the processes occurring in supernovae of type II (core-collapsing supernovae, CCSN) may be formulated as follows.

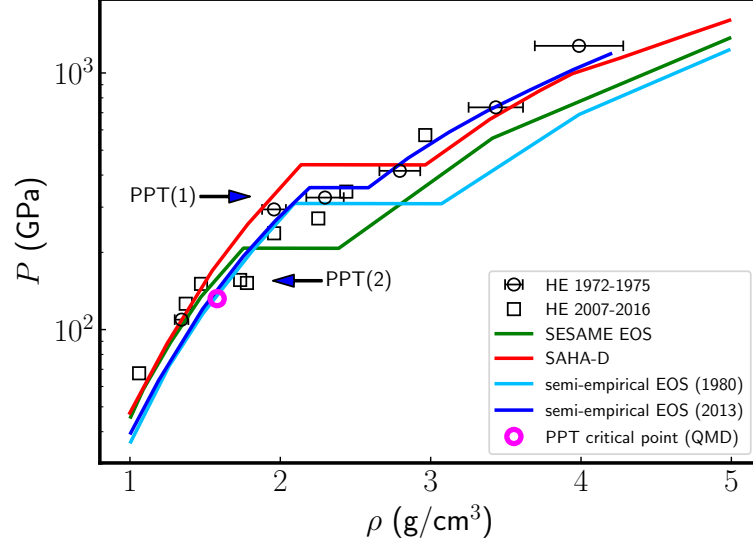


Figure 5: Hypothetical phase transition in quasi-isentropic HE-driven compression experiments (1972–2017) and in “cold” (low entropy) theoretical models. Experiment: hollow circles, quasi-isentropic VNIIEF 1972–1975 [17, 18]; rectangles – quasi-isentropic compression 2007–2017 [16, 26]; arrows, phase-transition-like discontinuities (1) in Refs. [17, 18] and (2) in Refs. [16, 26] supposed as “plasma” phase transitions (PPT). Calculation results: green, isotherm $T = 0$ K from EOS SESAME [32]; red line, isotherm $T = 300$ K from SAHA EOS [31] (“chemical picture”); light blue and blue, isotherm $T = 0$ K from two “wide-range” semiempirical EOSes: Refs. [33] and [34] correspondingly. Magenta circle, critical point of first-order liquid-liquid phase transition via *ab initio* QMD.

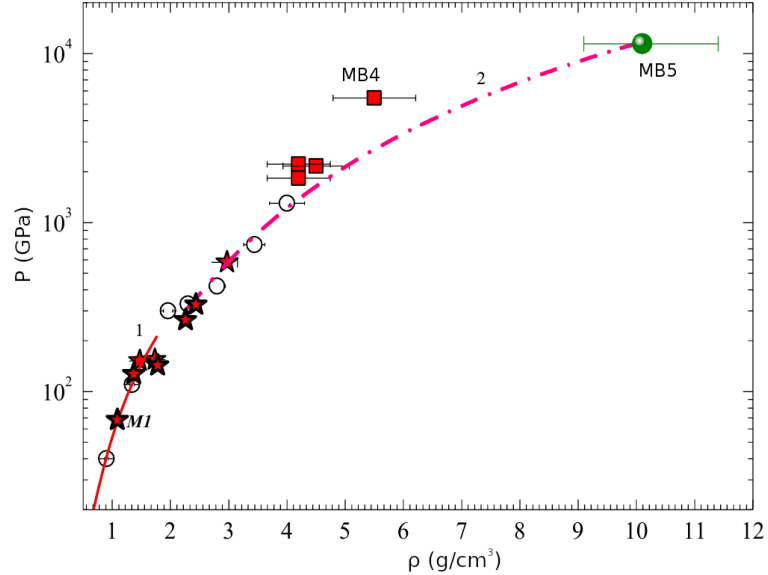


Figure 6: Two isentropes: 1 is the isentropic curve from the point M1 with the use of VNIIEF EOS for deuterium, and 2 is the isentrope based on SAHA-EOS from Fig. 15 in Ref. [26] above 150 GPa, which miraculously enters a new point MB5.

With the specially selected geometry of the experiment and the explosion intensity one can ensure that at the final stages of compression (“collapse”) of the steel shell the thermodynamic trajectory of the compressed deuterium would start entering the two-phase domain of the phase transition. When the central portion of the deuterium enters the two-phase zone, the EOS of the deuterium plasma becomes soft and the rate of the shell braking stops growing. The shell is still being compressed (“pushed”) by the products of explosion from outside, and it is accelerating. At the moment when the whole deuterium gas enters the phase of a strongly degenerate plasma, the stiffness of the deuterium plasma increases abruptly, and the rate of the shell braking grows strongly. A shock wave will run out into the pushing shell, which will cause a rarefaction Riemann wave on the outer boundary and perhaps even a “spallation” of the

surface. There will be a “rebound” (or just bounce) of the shell. In principle, this picture may be observed in γ -rays probing the dynamics of the whole process.

IV. STELLAR COLLAPSE SIMULATION

The death of massive stars is associated with one of the most striking events in the universe: a supernova explosion. The inner part of stellar core collapses to nuclear density, where the nuclear EOS stiffens due to the repulsive core of the nuclear force [37]. Collapse is halted abruptly on a millisecond timescale. The core of a newly born protoneutron star overshoots its new equilibrium and then bounces back (“core bounce”) into the still-infalling outer core, creating a shock wave. This shock first moves out dynamically but quickly loses energy by work done to dissociate the infalling iron-group nuclei into neutrons, protons, and α particles and also by the copious emission of neutrinos.

Many simulations of core-collapsing supernovae show that bounce pushes the shock wave, but later it *stalls*. Revival of the shock is needed for a successful explosion and it is the most important problem in SNe that should be solved in the future. The physics of shock revival is not reflected in experiments that we describe, but a study of the bounce with a laboratory tool that we propose is essential, as this stage forms initial conditions for the shock stalling and revival stages.

For a successful explosion to occur, the *supernova mechanism* must revive the shock within 1 s. Otherwise, the steady accretion stream of outer core and shell material will push the protoneutron star over its maximum mass (set by the nuclear EOS) and black-hole formation results (see, e.g., Ref. [38]). The primary candidate mechanism for driving typical CCSN explosions is the *neutrino mechanism* [39–42]. Neutrinos dominate CCSN energetics. The essence of the neutrino mechanism is that a fraction ($\sim 10\%$) of the outgoing $\nu_e + \bar{\nu}_e$ luminosity is deposited in a heating region behind the front of the stalled shock. This offsets the balance between the accretion ram pressure and the total pressure behind the shock, eventually leading to a runaway explosion [43]. However, the neutrino mechanism *fails* to explode ordinary massive stars in spherical symmetry (1D). Extensive work [44–49] in axisymmetry (2D) and in 3D has shown that multidimensional (multi-D) fluid dynamics may play a crucial role in the explosion mechanism.

The dynamics of the explosive experiment described above is similar in some aspects to the process of collapse during supernova explosions. Here we present the results of our modeling of a “standard” collapse which we will use for the illustration of our base analogy. We start from a $2M_\odot$ stellar iron core at the verge of its dynamical stability (i.e. the average adiabatic index $\langle \gamma \rangle$ is slightly less than $4/3$). The core is divided into 1000 nonequally spaced Lagrangean mass zones. The description of hydrodynamic equations solver used in this paper is given in Ref. [50]. It is based on a number of routines, first developed by D. Nadyozhin and extensively used in various astrophysical applications, ranging from core-collapse simulations [51–53] to low-mass neutron star explosion processes [54]. After some additional modifications, this solver now is a 1D, Newtonian, fully implicit Lagrangean FORTRAN code. It uses an artificial viscosity algorithm in a shock-capturing scheme when the shock is “smeared” onto three mesh cells. This simple approach appears, nevertheless, to be quite adequate when compared to much more sophisticated methods, see, e.g., Ref. [55].

The matter at the subnuclear domain is assumed to be under nuclear statistical equilibrium conditions, and the equation of state is taken according to Ref. [56]. For the electron-positron plasma with the blackbody equilibrium radiation EOS part we use the code EPEOS [57]. In the high-density domain, the effects of nonideality are included according to the excluded volume approximation [58]. For uniform nuclear matter, formed at densities $\rho \geq 10^{14}$ g/ccm, we use Lattimer–Swesty type EOS parametrization [59].

The most important part of the supernova simulation procedure, the neutrino transport scheme, is divided into two parts: for the inner opaque stellar core domain we use neutrino heat conduction (NHC) theory, first developed in Ref. [60] with additional scattering effects [61] included. For the outer semiopaque and transparent domain we use the scheme proposed in Ref. [62] with a few modifications [50], which ensure the smooth transition to the diffusion (NHC) limit.

Using our one-dimensional code, described above, we have obtained the trajectories of matter inside the collapsing star; see Fig. 7. The dynamics here is shown with so-called mass coordinates m , i.e., the mass enclosed by the radius r (the relation to ordinary coordinates is simple: $dm/dr = 4\pi r^2 \rho$, ρ is the matter density). We show the evolution of fixed Lagrangean masses $m = 0.3 \div 1.6 M_\odot$ (with $0.1 M_\odot$ step) in the time interval $-15 \leq t \leq 15$ ms around the bounce (zero time). The dashed line, connecting the empty circles, shows the position of the shock. Behind the shock, the matter is only slightly compressed, forming a quasiequilibrium configuration: a hot newborn neutron star.

The lower-left corner of the figure contains the zoomed-in part of the main image for a reduced time interval around the bounce and $m = 0.3 \div 0.7 M_\odot$. Curves here are divided into two types of behavior: for $m \leq 0.5$ they are smooth, and the matter is slightly overcompressed and comes to a new equilibrium state. For $m \geq 0.6$ we see a “kink”. Such a difference signifies the appearance of the shock wave somewhere between $m = 0.5$ and $m = 0.6$ (see also discussion of Fig. 9). For this and higher values of m the matter falls until it meets the shock front and is accelerated sharply:

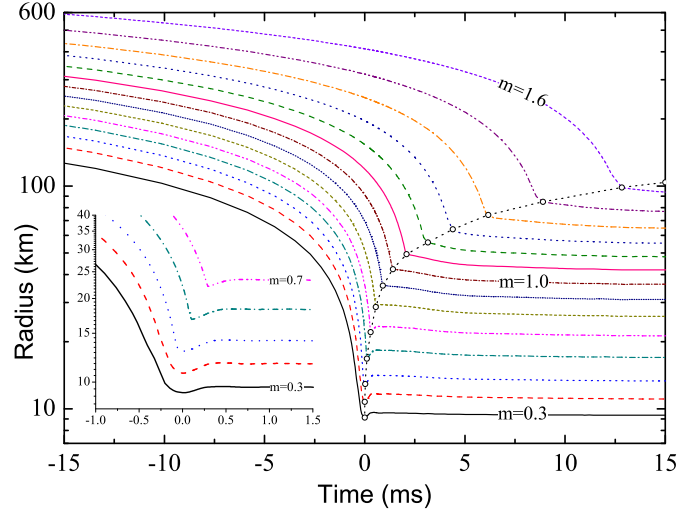


Figure 7: Evolution of radius coordinates during collapse and bounce for a protoneutron star at several fixed Lagrangean masses $m = 0.3 \div 1.6 M_{\odot}$ (with $0.1 M_{\odot}$ step). A dashed line, which connects empty circles, shows the position of the shock. The lower-left corner of figure contains the zoomed-in part of the main image for the reduced time interval around the bounce and $m = 0.3 \div 0.7 M_{\odot}$.

this leads to the formation of the “kink” in the enlarged pattern of the flow.

All of this is very similar to Fig. 4 where snapshots of the record high compression of the deuterium gas is reproduced. The comparison of this figures illustrate our base idea: the qualitative similarity between these two, in principle very different, processes.

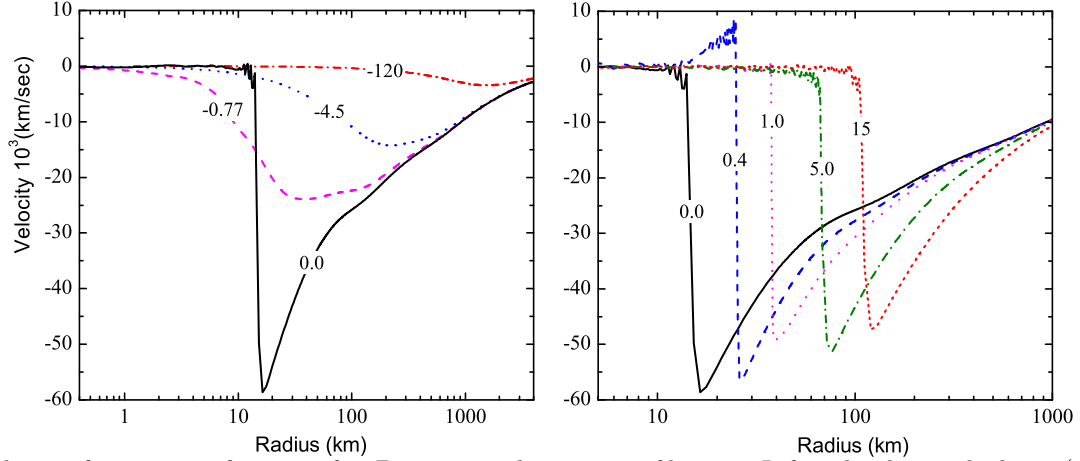


Figure 8: Velocity of matter as a function of r . Zero time is the moment of bounce. Left and right panels show $v(r)$ for different moments before and after the bounce correspondingly. The value of t (in ms) is shown on each curve.

To show the process of collapse from another point of view, we plot in Fig. 8 the velocity of matter v as a function of Eulerian coordinate r for different moments of time before (left panel) and after (right) the bounce. The moment $t = 0$ corresponds to the bounce itself, and time (in ms) is shown by numbers on each curve. The shock wave is formed at 15 km approximately and starts to propagate outwards. At $t = 0.4 \text{ ms}$ after bounce the velocity behind the shock is positive, but soon the shock is converted into an accreting, although still expanding, one. By the moment $t = 1 \text{ ms}$ it moves to $r \approx 40 \text{ km}$, then expands to $r \approx 70 \text{ km}$ at $t = 5 \text{ ms}$ and at the last moment shown, $t = 15 \text{ ms}$, the shock is situated at $r = 110 \text{ km}$ approximately. Thus it decelerates and later this outward moving shock wave stalls and is transformed into the standing accretion shock. Naturally, the only mechanism of bounce is not sufficient for the explosion to occur. Additional physics is required to revive this shock wave: neutrino contribution, multidimensional effects in the flow, or others. This problem is actively discussed in the literature [39–42, 44–49]. But, as mentioned above, the physics of the stalled shock revival is not reflected in the experiments described in the current paper.

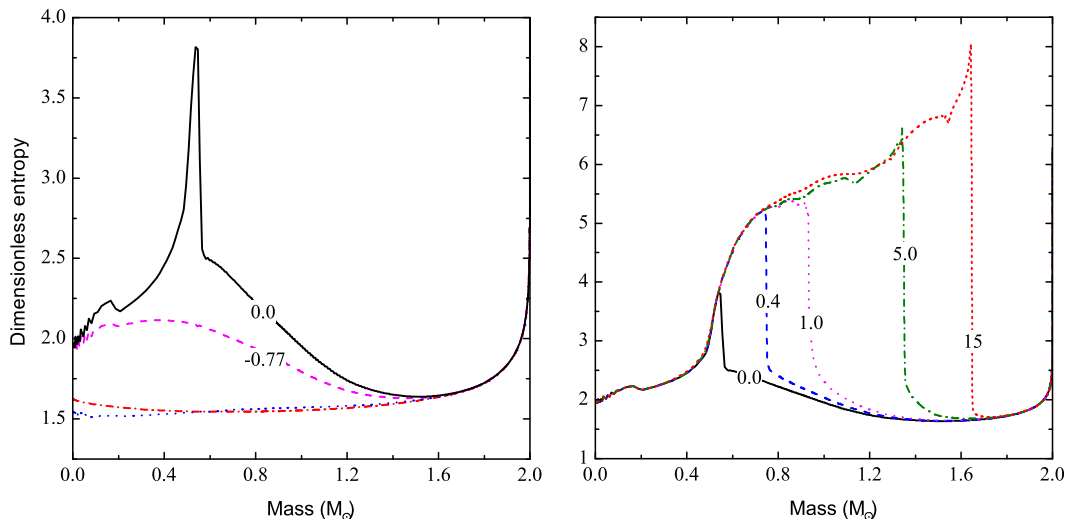


Figure 9: Entropy in the collapsing core. Left panel shows entropy profiles as a function of Lagrangean mass m before the bounce and the right panel after. The moments of time are the same, as in Fig. 8.

Another important similarity between explosive experiments and core-collapse process is the low-entropy matter conditions. Table II (last column) shows the dimensionless entropy of deuterium plasma at the time of maximum compression in our *quasi-isentropic* experiments. Now we can compare these data to the entropy values, reached during supernova explosion.

Figure 9 shows dimensionless entropy per baryon in the collapsing stellar core for the same collapse model as in Figs. 7 and 8. Left and right panels show the entropy profiles as a function of Lagrangean mass before and after the bounce respectively. The moments of time are the same, as in Fig. 8. One can see that before the bounce the entropy grows moderately until the shock is formed at $m \approx 0.55 M_\odot$ (see the discussion of the Fig. 7 above). Shock starts to propagate through the falling matter and heats it up. But even behind the shock the values of entropy of matter are close by the order of magnitude to the experimental results from Table II. Thus we can conclude that the low-entropy condition is really another important similarity which connects stellar physics and our terrestrial experiments.

V. SUMMARY AND DISCUSSION

The experiments presented in the paper reveal the analogy between explosive experiments for high compression of matter and the dynamics of supernova collapses.

Let us point out which features of stellar core-collapse can be modeled by the experiments of the same class as described in this paper.

- The analogy is based on the similarity of the dynamics: in both systems a close-to-spherical compression occurs, the central region equation of state stiffens, and this leads to the bounce.
- The important feature of the experiments is that all dynamics happens at low entropy: the entropy value shows the relative contribution to the EOS of the cold part of matter, so the role of EOS changing in the bounce process in laboratory reveals that in supernovae.
- The experimentally observed phase transition of the first kind and softening of EOS may be relevant for understanding the exotic mechanisms of supernova explosions, where a phase transition may occur. The phase transitions which are plausible in SN dynamics [63] may help to produce a successful supernova [64] in the process of evolution of massive progenitors.
- The development of 3D hydrodynamic instabilities may be studied in future experiments with controlled initial asymmetric perturbations and/or addition of magnetic fields.
- Finally, the spallation of the surface of compressed samples after the bounce is similar to another phenomenon already observed in supernovae, namely, the so-called shock breakout [65–67].

The reader should be aware that we are able to model only a limited subset of phenomena occurring in a real stellar collapse. The following features are not reproduced in HE experiments:

- Neutrino emission.
- Dissociation of nuclei by shock waves.
- Shock wave stalling in the accretion flow.
- Gravity and General Relativity (GR) effects.

The goal of our paper is to emphasize the analogy and to present such experiments as a new platform for laboratory astrophysics. Consequently, the experiments of this kind expand the possibilities and the list of existing laboratory astrophysics platforms (for a review see [4, 8]), among which we could highlight the following.

- High-compression experiments (see, e.g., Refs. [68, 69]) that study equations of state in conditions similar to interiors of giant planets.
- Laboratory and numerical experiments on hydrodynamic instabilities and opacity measurements in relation to stellar and supernova physics [8, 70, 71].
- Experiments on collisionless physics of gaseous supernova remnants (e.g. collisionless shock waves) [72].

It should be pointed out that previous work on laboratory astrophysics of core-collapsing supernovae was concentrated more on problems of Rayleigh-Taylor and Richtmyer-Meshkov instabilities in the supernova shocks [8, 70, 71]. More recent work is done on the simulations growth of instabilities in the collapse phase, see Ref. [73] and references and citations therein.

Our paper presents a new record of compression in laboratory high explosive experiments. The pressure obtained in experiments of another type, namely, laser facilities, e.g. NIF [74], may be higher, approaching $P \sim 100$ Gbar, but at significantly smaller spatial scales and short lifetimes. The explosive experiment described by us reaches maximum pressure at $l_{\text{expl}} \sim 1$ cm scale and $t_{\text{expl}} \sim 1 \mu\text{s}$ (cf. Fig. 4), while for laser facilities these numbers are $l_{\text{las}} \sim 10 \mu\text{m}$ scale and $t_{\text{expl}} \sim 0.1 - 1$ ns. The latter significantly complicates the diagnostics. The larger scale of explosion-driven compression allows one to get much more details [1–4] of the hydrodynamic flows and shocks.

The goal of our paper is not to give an exhaustive review of the current status of core-collapse simulations with successful and unsuccessful SN explosions (see Refs. [44–49] and the papers citing them).

One may ask, Are there any scenarios in which one might expect the shock generated in the HE experiment to “fail” and would there be any secondary indications of this failure on the plasma properties? In fact, our experiments allow us to model only a limited number of properties. The shocks propagating in the compressed material are not stalled by the energy losses due to dissociation of heavy nuclei and huge neutrino emission from the downstream region, as is envisaged in supernovae. Those features are not possible to model in the HE experiments. However, even the narrow range of properties in the experiment is useful for understanding the flows in nonideal plasma which are initially spherically symmetric with a high degree of accuracy during the compression phase and later develop 3D asymmetries at the expansion stage.

There have been suggestions that even failed supernovae can give rise to the secondary indications of the collapse: weak shocks and outbursts (e.g., Refs. [75, 76]). These conclusions are relevant for more realistic situations when neutrinos take away a lot of energy from the collapsing core. Nevertheless, those neutrino losses occur on a long diffusion timescale (seconds in the star core), while the bounce of the stellar core goes on a much shorter timescale (milliseconds) after neutrinos are trapped. Thus, the pattern of hydro flows is very similar in our experiments and in the simulations of the stellar core bounce.

The recent progress in supernova theory shows, that even collapses which do not lead to a prompt supernova explosion may have bright manifestations due to a fallback energy release, see Refs. [77, 78]. Reference [78] not only develops a physical model of mass ejection in failed supernovae but also advances a self-similar solution applicable for those events. In future work, self-similar solutions of this type may be tried also for the description of hydrodynamic flows in experiments discussed here (cf. the results on self-similar volume compression in laser fusion conditions [79]).

VI. CONCLUSIONS

The similarity in dynamics seen in Figs. 4 and 7 is a basic analogy, which can conceptually relate thermal and fluid dynamics in explosive experiments with the processes occurring in type Ib/c and type II supernovae (CCSN) and permits us to use the explosive experiment as a laboratory site to study hydrodynamics of the collapse and bounce. Not only a new dimension for laboratory astrophysics is open by the new experiments but also a new tool appears for validation of codes used in applied science and in astrophysics.

The simulations of explosive experiments with a hydrodynamic code that describes the dynamics of the whole structure, the steel shell, the gas-target, and high explosive and detonation products, agrees well with the results of the experiment. An important part of the simulations are equations of state, that describe all transitions that occur within the material being investigated. As was emphasized above, these transitions are crucial for the proposed analogy between supernovae and explosive experiment. The equations of state used in experiment description are the realization of theoretical models [3, 4], which is published elsewhere [26]. Another important feature of the experiment is the low entropy regime of compression, this fact brings the experiments closer to the condition in real supernovae, where entropy of the collapsing material is also quite low.

We conclude that such an experimental tool opens new horizons in laboratory astrophysics. It allows one to study the process of collapse: the compressed matter mimics this astrophysical phenomenon. High pressures together with low entropy lead to degeneracy of plasma and, therefore, simulate the stiffness of the equation of state in a real collapsing star, leading to the bounce of the shell. This process is an inevitable part of collapse and its hydrodynamics can now be studied in laboratory. Full control of initial conditions in laboratory gives a possibility to investigate the role of additional effects on the hydrodynamics of collapse, e.g. perturbations that violate the spherical symmetry of the system (this resembles asymmetries in initial star configuration, like rotation, magnetic field, etc.).

Acknowledgments

We are grateful to V.E.Fortov for the idea to use HE experiments in laboratory astrophysics of bounce in core-collapsing supernovae and to anonymous referees for valuable comments.

This research was partially supported by Russian Science Foundation Grant No. 16-12-10519 (S. Glazyrin) and Grant No. 18-12-00522 (S. Blinnikov).

-
- [1] R. J. Hemley and N. W. Ashcroft, *Physics Today* **51**, 26 (1998).
 - [2] R. Drake, *High-Energy-Density Physics* (Springer-Verlag Berlin Heidelberg, 2006).
 - [3] V. Fortov, *Extreme States of Matter: High Energy Density Physics* (Springer International Publishing, 2016).
 - [4] V. Fortov, *Thermodynamics and Equations of State for Matter: From Ideal Gas to Quark-Gluon Plasma* (World Scientific Publishing Co, 2016).
 - [5] D. Henderson, *Frontiers in High Energy Density Physics* (Washington: National Research Council, Nat. Acad. Press, 2003).
 - [6] B. A. Remington, R. E. Rudd, and J. S. Wark, *Physics of Plasmas* **22**, 090501 (2015).
 - [7] J.-P. Davis, M. D. Knudson, and J. L. Brown, in *American Institute of Physics Conference Series* (2017), vol. 1793 of *American Institute of Physics Conference Series*, p. 060015.
 - [8] B. A. Remington, R. P. Drake, and D. D. Ryutov, *Reviews of Modern Physics* **78**, 755 (2006).
 - [9] M. A. Mochalov, R. I. Il'kaev, V. E. Fortov, A. L. Mikhailov, V. A. Arinin, A. O. Blikov, V. A. Komrakov, I. P. Maksimkin, V. A. Ogorodnikov, and A. V. Ryzhkov, *Pis'ma ZhETP* **107**, 173 (2018).
 - [10] H.-T. Janka, *Handbook of Supernovae*, Alsabti, A. W., Murdin, P. (Eds.) (2017), arXiv:1702.08825.
 - [11] N. W. Ashcroft, *Nature* (London) **340**, 345 (1989).
 - [12] N. W. Ashcroft, in *High Pressure Phenomena*, edited by G. L. Chiarotti, R. Hemley, M. Bernasconi, and L. Ulivi (IOS Press, Amsterdam, 2002), p. 151.
 - [13] W. J. Nellis, S. T. Weir, and A. C. Mitchell, *Phys. Rev. B* **59**, 3434 (1999).
 - [14] V. Y. Ternovoi, A. S. Filimonov, V. E. Fortov, S. V. Kvitov, D. N. Nikolaev, and A. A. Pyalling, *Physica B Condensed Matter* **265**, 6 (1999).
 - [15] V. Y. Ternovoi, A. S. Filimonov, A. A. Pyalling, V. B. Mintsev, and V. E. Fortov, in *Shock Compression of Condensed Matter*, edited by M. D. Furnish, Y. Horie, and N. N. Thadhani (2002), vol. 620 of *American Institute of Physics Conference Series*, pp. 107–110.
 - [16] M. A. Mochalov, R. I. Il'kaev, V. E. Fortov, A. L. Mikhailov, Y. M. Makarov, V. A. Arinin, S. K. Grishechkin, A. O. Blikov, V. A. Ogorodnikov, A. V. Ryzhkov, et al., *Journal of Experimental and Theoretical Physics Letters* **92**, 300 (2010).
 - [17] D. K. Grigoriev, S. Kormer, and others, *Pis'ma ZhETP* **16**, 286 (1972).
 - [18] D. K. Grigoriev, S. Kormer, and others, *ZhETP* **69**, 743 (1975).
 - [19] S. G. Brush, H. L. Sahlin, and E. Teller, *J. Chem. Phys.* **45**, 2102 (1966).
 - [20] H. M. Van Horn, *Physics Letters A* **28**, 706 (1969).
 - [21] W. L. Slattery, G. D. Doolen, and H. E. Dewitt, *Phys. Rev. A* **21**, 2087 (1980).
 - [22] D. G. Yakovlev and D. A. Shalybkov, *Astrophysics and Space Physics Reviews* **7**, 311 (1989).
 - [23] S. I. Glazyrin and S. I. Blinnikov, *Journal of Physics A* **43**, 075501 (2010), arXiv:0907.0439.
 - [24] V. E. Fortov, R. I. Ilkaev, V. A. Arinin, V. V. Burtzev, V. A. Golubev, I. L. Iosilevskiy, V. V. Khrustalev, A. L. Mikhailov, M. A. Mochalov, V. Y. Ternovoi, et al., *Physical Review Letters* **99**, 185001 (2007).

- [25] M. A. Mochalov, R. I. Il'kaev, V. E. Fortov, A. L. Mikhailov, V. A. Arinin, A. O. Blikov, V. A. Komrakov, A. V. Ryzhkov, V. A. Ogorodnikov, and A. A. Yukhimchuk, *Journal of Experimental and Theoretical Physics Letters* **101**, 519 (2015).
- [26] M. A. Mochalov, R. I. Il'kaev, V. E. Fortov, A. L. Mikhailov, A. O. Blikov, V. A. Ogorodnikov, V. A. Gryaznov, and I. L. Iosilevskiy, *Journal of Experimental and Theoretical Physics, JETP* **124**, 505 (2017).
- [27] R. Ilkaev and V. Fortov, *Experiments on record high-explosive quasi-isentropic compression of deuterium up to 110 mbar*, Oral talk at Presidium of Russian Academy of Sciences Session on December 20 (2016).
- [28] V. E. Fortov, *Physics Uspekhi* **52**, 615 (2009).
- [29] A. I. Pavlovskii, G. D. Kuleshov, G. V. Sklizkov, Y. A. Zysin, and A. I. Gerasimov, *Soviet Physics Doklady* **10**, 30 (1965).
- [30] N. I. Egorov, G. V. Boriskov, A. I. Bykov, Y. P. Kuropatkin, N. B. Lukyanov, V. D. Mironenko, and V. N. Pavlov, *Contributions to Plasma Physics* **51**, 333 (2011).
- [31] V. K. Gryaznov and I. L. Iosilevskiy, *Journal of Physics A Mathematical General* **42**, 214007 (2009).
- [32] G. I. Kerley, *A Theoretical Equation of State for Deuterium*, LASL Scientific Report LA-4776 (1972).
- [33] V. P. Kopyshev and V. V. Khrustalev, *PMTF* **21**, 122 (1980).
- [34] V. D. Urlin, *Soviet Journal of Experimental and Theoretical Physics* **117**, 833 (2013).
- [35] A. V. Chentsov and P. R. Levashov, *Contributions to Plasma Physics* **52**, 33 (2012).
- [36] W. Lorenzen, B. Holst, and R. Redmer, *Phys. Rev. B* **82**, 195107 (2010).
- [37] H. A. Bethe, *Rev. Mod. Phys.* **62**, 801 (1990).
- [38] E. O'Connor and C. D. Ott, *Astrophys. J.* **730**, 70 (2011).
- [39] S. A. Colgate and M. H. Johnson, *Phys. Rev. Lett.* **5**, 235 (1960).
- [40] W. D. Arnett, *Canadian Journal of Physics* **44**, 2553 (1966).
- [41] D. K. Nadyozhin, *Astrophys. Space Sci.* **53**, 131 (1978).
- [42] H.-T. Janka, *Ann. Rev. Nuc. Par. Sci.* **62**, 407 (2012), 1206.2503.
- [43] H. A. Bethe and J. R. Wilson, *Astrophys. J.* **295**, 14 (1985).
- [44] R. Buras, H.-T. Janka, M. Rampp, and K. Kifonidis, *Astron. & Astrophys.* **457**, 281 (2006).
- [45] C. D. Ott, A. Burrows, L. Dessart, and E. Livne, *Astrophys. J.* **685**, 1069 (2008).
- [46] B. Müller, H.-T. Janka, and A. Heger, *Astrophys. J.* **761**, 72 (2012), 1205.7078.
- [47] S. W. Bruenn, E. J. Lentz, W. R. Hix, A. Mezzacappa, J. A. Harris, O. E. B. Messer, E. Endeve, J. M. Blondin, M. A. Chertkow, E. J. Lingerfelt, et al., *Astrophys. J.* **818**, 123 (2016), 1409.5779.
- [48] E. J. Lentz, S. W. Bruenn, W. R. Hix, A. Mezzacappa, O. E. B. Messer, E. Endeve, J. M. Blondin, J. A. Harris, P. Marronetti, and K. N. Yakunin, *Astrophys. J. Letters* **807**, L31 (2015), 1505.05110.
- [49] S. M. Couch and C. D. Ott, *Astrophys. J.* **799**, 5 (2015), 1408.1399.
- [50] A. V. Yudin, *Physical processes inside collapsing stellar cores*, PhD thesis (2009).
- [51] L. N. Ivanova, V. S. Imshennik, and D. K. Nadezhin, *Nauchnye Informatsii* **13**, 3 (1969).
- [52] D. K. Nadezhin, *Astrophys. Space Sci.* **49**, 399 (1977).
- [53] D. K. Nadezhin, *Astrophys. Space Sci.* **51**, 283 (1977).
- [54] S. I. Blinnikov, V. S. Imshennik, D. K. Nadezhin, I. D. Novikov, T. V. Perevodchikova, and A. G. Polnarev, *Soviet Astronomy* **34**, 595 (1990).
- [55] A. G. Tolstov, S. I. Blinnikov, and D. K. Nadyozhin, *Mon. Not. of the Royal Astro. Soc.* **429**, 3181 (2013), 1212.3662.
- [56] D. K. Nadyozhin and A. V. Yudin, *Astronomy Letters* **30**, 634 (2004).
- [57] S. I. Blinnikov, N. V. Dunina-Barkovskaya, and D. K. Nadyozhin, *Astrophys. J. Suppl.* **106**, 171 (1996).
- [58] A. V. Yudin, *Astronomy Letters* **37**, 576 (2011), 1406.3148.
- [59] J. M. Lattimer and F. Douglas Swesty, *Nuclear Physics A* **535**, 331 (1991).
- [60] V. S. Imshennik and D. K. Nadezhin, *Zhurnal Eksperimentalnoi i Teoreticheskoi Fiziki* **63**, 1548 (1972).
- [61] A. V. Yudin and D. K. Nadyozhin, *Astronomy Letters* **34**, 198 (2008).
- [62] D. K. Nadezhin and I. V. Otroshchenko, *Soviet Astronomy* **24**, 47 (1980).
- [63] I. Sagert, T. Fischer, M. Hempel, G. Pagliara, J. Schaffner-Bielich, A. Mezzacappa, F.-K. Thielemann, and M. Liebendörfer, *Physical Review Letters* **102**, 081101 (2009), arXiv:0809.4225.
- [64] T. Fischer, N.-U. F. Bastian, M.-R. Wu, P. Baklanov, E. Sorokina, S. Blinnikov, S. Typel, T. Klähn, and D. B. Blaschke, *Nature Astronomy* **2**, 980 (2018), arXiv:1712.08788.
- [65] K. Schawinski, S. Justham, C. Wolf, P. Podsiadlowski, M. Sullivan, K. C. Steenbrugge, T. Bell, H.-J. Röser, E. S. Walker, P. Astier, et al., *Science* **321**, 223 (2008), 0803.3596.
- [66] S. Gezari, D. O. Jones, N. E. Sanders, A. M. Soderberg, T. Hung, S. Heinis, S. J. Smartt, A. Rest, D. Scolnic, R. Chornock, et al., *Astrophys. J.* **804**, 28 (2015), 1502.06964.
- [67] P. M. Garnavich, B. E. Tucker, A. Rest, E. J. Shaya, R. P. Olling, D. Kasen, and A. Villar, *Astrophys. J.* **820**, 23 (2016), 1603.05657.
- [68] H. Azechi, T. Jitsuno, T. Kanabe, M. Katayama, K. Mima, N. Miyanaga, M. Nakai, S. Nakai, H. Nakaishi, M. Nakatsuka, et al., *Laser and Particle Beams* **9**, 193 (1991).
- [69] H. Azechi, in *Journal of Physics Conference Series* (2016), vol. 717 of *Journal of Physics Conference Series*, p. 012119.
- [70] A. L. Velikovich, J. P. Dahlburg, A. J. Schmitt, J. H. Gardner, L. Phillips, F. L. Cochran, Y. K. Chong, G. Dimonte, and N. Metzler, *Physics of Plasmas* **7**, 1662 (2000).
- [71] Y. Zhou, B. A. Remington, H. F. Robey, A. W. Cook, S. G. Glendinning, A. Dimits, A. C. Buckingham, G. B. Zimmerman, E. W. Burke, T. A. Peyser, et al., *Physics of Plasmas* **10**, 1883 (2003).
- [72] H.-S. Park, D. Higginson, C. Huntington, B. Pollock, B. Remington, H. Rinderknecht, J. Ross, D. Ryutov, G. Swadling, S. Wilks, et al., in *APS Meeting Abstracts* (2017), p. CO5.002.

- [73] C. C. Jøggerst, A. Nelson, P. Woodward, C. Lovekin, T. Masser, C. L. Fryer, P. Ramaprabhu, M. Francois, and G. Rockefeller, *Journal of Computational Physics* **275**, 154 (2014).
- [74] O. A. Hurricane, D. A. Callahan, D. T. Casey, E. L. Dewald, T. R. Dittrich, T. Döppner, S. Haan, D. E. Hinkel, L. F. Berzak Hopkins, O. Jones, et al., *Nature Physics* **12**, 800 (2016).
- [75] D. K. Nadezhin, *Astrophys. Space Sci.* **69**, 115 (1980).
- [76] E. Lovegrove and S. E. Woosley, *Astrophys. J.* **769**, 109 (2013), arXiv:1303.5055.
- [77] T. J. Moriya, G. Terreran, and S. I. Blinnikov, *Mon. Not. of the Royal Astro. Soc.* **475**, L11 (2018), arXiv:1712.02579.
- [78] E. R. Coughlin, E. Quataert, R. Fernández, and D. Kasen, *Mon. Not. of the Royal Astro. Soc.* **477**, 1225 (2018), arXiv:1710.01746.
- [79] H. Hora, H. Azechi, Y. Kitagawa, K. Mima, M. Murakami, S. Nakai, K. Nishihara, H. Takabe, C. Yamanaka, M. Yamanaka, et al., *Journal of Plasma Physics* **60**, 743 (1998).

Table I: Parameters of deuterium plasma compressed by pressure $P \approx 11400$ GPa (experimental values and simulation with VNIIEF EOS)

run	R_0 , mm	R_{\min} , mm	ρ_0 , g/cm ³	ρ_{exp} , g/cm ³	P_{calc} , GPa	ρ_{calc} , g/cm ³	T_{calc} , kK
MB5	31	4.74	0.0354	$10.1^{+1.3}_{-0.9}$	11400^{+2000}_{-2000}	11.1	36.5

Table II: Deuterium plasma state at the time of maximum compression in quasi-isentropic compression experiments (Vserossiiskiy Nauchno-Issledovatel'skiy Institut Experimental'noi Fiziki, VNIIEF, Sarov), calculated using EOS SAHA. Given are values of pressure P , density ρ , temperature T , degeneracy parameter for free electrons $\xi = n_e \lambda^3$ (2.3), and specific entropy S (per gram and per nucleon)

run	P , GPa	ρ , g/cm ³	T , kK	$n_e \lambda^3$	S , J/g·K	S , 1/ k_B
1	68	1.07	2.15	—	22.2	2.67
2	127	1.35	2.49	8.04	23.5	2.83
3	143	1.76	2.60	9.6	—	—
4	265	2.2	4.52	60.5	29.4	3.53
5	327	2.37	6.30	54.7	31.8	3.82
6	583	2.91	6.85	66.3	30.9	3.72
7	1830	4.2	19.71	36.0	37.6	4.52
8	2215	4.2	31.50	21.4	41.8	5.03
9	2160	4.5	21.15	35.9	37.7	4.53
10	5450	5.5	69.16	11.4	46.8	5.63
MB5	11400^{+2000}_{-2000}	11.1	36.5	—	34.5	4.15
NIF	$1.4 \cdot 10^7$	30	$5 \cdot 10^4$	—	117	14.1